The seasonal cycle of carbonate system processes in Ryder Bay, West Antarctic Peninsula

Oliver J. Legge[a,*], Dorothee C.E. Bakker[a], Michael P. Meredith[b], Hugh J. Venables[b], Peter J. Brown[c], Elizabeth M. Jones[d], Martin T. Johnson[e]

[a] Centre for Ocean and Atmospheric Sciences, School of Environmental Sciences, University of East Anglia, Norwich Research Park, Norwich NR4 7TJ, UK
[b] British Antarctic Survey, High Cross, Madingley Road, Cambridge CB3 0ET, UK
[c] National Oceanography Centre, Waterfront Campus, European Way, Southampton SO14 3ZH, UK
[d] Centre for Energy and Environmental Sciences, Energy and Sustainability Research Institute Groningen, University of Groningen, Nijenborgh 4, 9747 AG Groningen, The Netherlands
[e] Centre for Environment Fisheries and Aquaculture Science, Lowestoft NR33 0HT, UK

ARTICLE INFO

ABSTRACT

The carbon cycle in seasonally sea-ice covered waters remains poorly understood due to both a lack of observational data and the complexity of the system. Here we present three consecutive seasonal cycles of upper ocean dissolved inorganic carbon (DIC) and total alkalinity measurements from Ryder Bay on the West Antarctic Peninsula. We attribute the observed changes in DIC to four processes: mixing of water masses, air–sea CO_2 flux, calcium carbonate precipitation/dissolution and photosynthesis/respiration. This approach enables us to resolve the main drivers of the seasonal DIC cycle and also investigate the mechanisms behind interannual variability in the carbonate system. We observe a strong, asymmetric seasonal cycle in the carbonate system, driven by physical processes and primary production. In summer, melting glacial ice and sea ice and a reduction in mixing with deeper water reduce the concentration of DIC in surface waters. The dominant process affecting the carbonate system is net photosynthesis which reduces DIC and the fugacity of CO_2, making the ocean a net sink of atmospheric CO_2. In winter, mixing with deeper, carbon-rich water and net heterotrophy increase surface DIC concentrations, resulting in pH as low as 7.95 and aragonite saturation states close to 1. We observe no clear seasonal cycle of calcium carbonate precipitation/dissolution but some short-lived features of the carbonate time series strongly suggest that significant precipitation of calcium carbonate does occur in the Bay. The variability observed in this study demonstrates that changes in mixing and sea-ice cover significantly affect carbon cycling in this dynamic environment. Maintaining this unique time series will allow the carbonate system in seasonally sea-ice covered waters to be better understood.

1. Introduction

The Southern Ocean plays an important role in the global carbon cycle through the uptake and storage of atmospheric CO_2 (Sabine et al., 2004) and the formation of deep water masses (Sallée et al., 2012). However, the role of the seasonally sea-ice covered coastal Southern Ocean in the global carbon cycle remains poorly constrained (Lenton et al., 2013) due to a scarcity of observations and the complexity and variability of this environment. If we are to predict future interactions between the changing climate and the carbon cycle in this environment, a better process-based understanding must be developed. The waters of the West Antarctic Peninsula (WAP) exhibit strong seasonal and interannual variability and are experiencing significant climate

change. This variability makes the region an ideal location to study carbon system processes and their interactions on various timescales. In the last fifty years the peninsula has seen a rapid increase in air temperature (Vaughan et al., 2003; Turner et al., 2005) and coincident changes in ocean temperature and stratification (Meredith and King, 2005). Most glaciers on the peninsula are retreating (Cook et al., 2005) and, unlike other parts of the Southern Ocean, the Antarctic Peninsula and southern Bellingshausen Sea have experienced a decrease in sea-ice cover (Stammerjohn et al., 2008; Comiso and Nishio, 2008; Parkinson and Cavalieri, 2012). Interannual to decadal variability in the atmospheric circulation of the region has also been observed. There has been a trend towards the positive phase of the Southern Annular Mode (SAM) over recent decades with a concordant intensification of

---
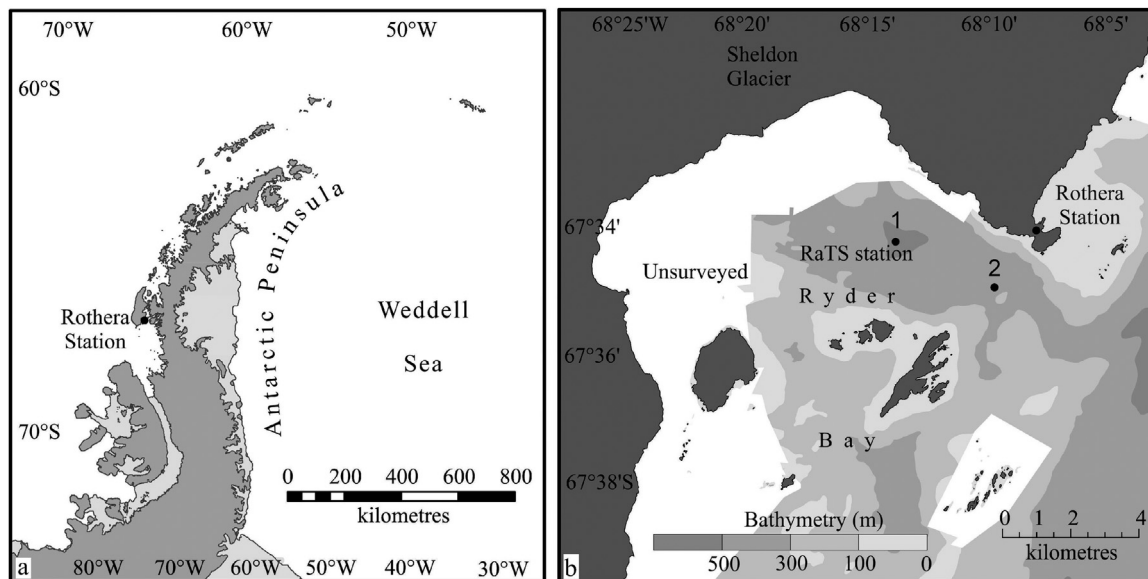
Fig. 1. (a) Location of Rothera on Adelaide Island at the West Antarctic Peninsula. (b) Location of RaTS sites 1 and 2 in Ryder Bay. From Legge et al. (2015), modified from Venables et al. (2013).

westerly winds (Thompson and Solomon, 2002; Marshall, 2003). The changes in wind are thought to be responsible for part of the observed warming on the peninsula (Marshall et al., 2006) and changes in ice dynamics in the region (Holland and Kwok, 2012). An increase in westerly wind stress may also lead to an increase in upwelling around the Antarctic continent (Hall and Visbeck, 2002), supplying more inorganic carbon to the surface ocean and thereby potentially weakening the strength of the Southern Ocean CO_2 sink (Lenton and Matear, 2007; Lovenduski et al., 2008; Le Quéré et al., 2007).

The global increase in atmospheric CO_2 leads to higher concentrations of CO_2 in the surface oceans with a concomitant decrease in pH and the concentration of carbonate ions, a process referred to as ocean acidification (Feely et al., 2004; Orr et al., 2005). The saturation state of calcium carbonate (Ω) describes the thermodynamic potential for this mineral to precipitate or dissolve and is calculated as the product of the concentrations of dissolved calcium and carbonate ions divided by their product at equilibrium. Wintertime undersaturation of the calcium carbonate mineral aragonite is predicted in the surface waters of the Southern Ocean by 2030 (McNeil and Matear, 2008) and the annual mean saturation state in the Southern Ocean is predicted to be less than 1 by the end of this century (Orr et al., 2005). The polar oceans are especially sensitive to ocean acidification as their low total alkalinity (TA) to dissolved inorganic carbon (DIC) ratio reduces their carbonate buffering capacity (Egleston et al., 2010; Shadwick et al., 2013).

Many marine organisms build calcium carbonate structures and there is growing concern over how ocean acidification may affect these organisms. Pteropods (Comeau et al., 2010; Bednaršek et al., 2012; Manno et al., 2012), foraminifera (Moy et al., 2009) and Antarctic krill (Kawaguchi et al., 2013) may be vulnerable to ocean acidification and resulting changes to their biomass, number and distribution could have significant ecological impacts. However, McNeil et al. (2011) observe that the natural seasonal variation in the saturation state of aragonite is large compared to the changes due to the uptake of anthropogenic CO_2 and suggest that Antarctic pteropods may be resilient to variations in Ω.

Due to the challenges of sampling in the polar environment, there are few measurements of the carbonate system from the coastal Southern Ocean and the vast majority of observations have been in the austral summer. Summer data from the Palmer Long-Term Ecological Research (Pal-LTER) grid show that carbonate chemistry on the WAP shelf is primarily influenced by primary production (Hauri

et al., 2015) which is known to be strongly influenced by wind and sea-ice conditions (Vernet et al., 2008; Montes-Hugo et al., 2009, 2010; Venables et al., 2013). In near-shore areas of the West Antarctic, freshwater inputs also affect carbonate chemistry through the dilution of carbonate ions. However, the influence of primary production dominates; biological CO_2 uptake increases the pH and the carbonate ion concentration, increasing Ω (Mattsdotter Björk et al., 2014; Hauri et al., 2015). Very few studies have observed a full seasonal cycle of inorganic carbon in the seasonally ice-covered Southern Ocean. Two full annual cycles of inorganic carbon have been characterised in Prydz Bay, East Antarctica (Gibson and Trull, 1999; Roden et al., 2013). These studies were separated by 15 years and showed the same general pattern of a build up of DIC under ice in winter followed by rapid biological drawdown of inorganic carbon in summer. However, significant differences between the two study periods were apparent, with higher DIC and lower pH in the more recent dataset which the authors attribute to a combination of ocean acidification and variations in primary production (Roden et al., 2013). This comparison highlights the challenges inherent in determining reliable decadal trends in a dynamic, sparsely sampled environment. Multi-year datasets from different locations are required to understand the drivers of the carbonate system and their changes in both time and space. Here, we present three consecutive seasonal cycles of DIC and TA measurements from a coastal time series on the WAP. We quantify carbonate system processes and investigate their seasonal and interannual variability.

2. Methods

2.1. Sampling and analysis

Samples for DIC and TA were collected between December 2010 and February 2014 at the Rothera Time Series (RaTS), about 4 km offshore, in Ryder Bay, on the West Antarctic Peninsula (Fig. 1). Sampling was undertaken from a rigid inflatable boat or through a hole in the ice approximately weekly in summer and every two weeks in winter, weather and ice permitting. If partial ice cover prevented access to the main RaTS site (site 1, Fig. 1) then a secondary site was used (site 2, Fig. 1). Most samples were taken at 15 m depth and some were taken at 40 m. Samples were collected in 250 mL or 500 mL borosilicate glass bottles, poisoned with mercuric chloride and sealed with

greased stoppers. They were transported back to the University of East Anglia, UK at the end of each field season for analysis. DIC was measured by coulometry (Johnson et al., 1985) following Standard Operating Procedure (SOP) 2 of Dickson et al. (2007) and TA was measured by potentiometric titration (Mintrop et al., 2000) following SOP 3b of Dickson et al. (2007). DIC and TA were measured using two VINDTAs (versatile instrument for the determination of titration alkalinity, version 3C, Marianda, Germany). The instruments were calibrated using certified reference materials from the Scripps Institution of Oceanography.

Sea-ice type and fraction of ice cover were visually estimated by marine assistants at Rothera. Fast ice is sea ice which is attached to land or to the front of a glacier. Brash ice consists of floating fragments, broken from other forms of sea ice. Temperature, salinity, fluorescence and pressure were measured during full depth (500 m at site 1) CTD casts. Discrete water samples were taken at 15 m depth for chlorophyll-a, macronutrients and salinity. For further details on sampling at RaTS see Venables et al. (2013) and Clarke et al. (2008). The mixed layer depth was defined as the depth at which density is 0.05 kg m^{-3} greater than at a reference depth (Venables et al., 2013). From November to April the sea surface was used as the reference depth but from May to October a reference depth of 10 m was used in order to prevent shallow, small scale meltwater events affecting the results. We also present a measure of stratification, defined as the energy (in J/m^2) that would be required to homogenise the top 100 m of the water column (Venables and Meredith, 2014).

The fugacity of CO_2 in water ($f$$CO_2$), the saturation state of the calcium carbonate minerals calcite and aragonite, and the pH were calculated from measurements of DIC, TA, temperature, salinity, silicate and phosphate using the CO2SYS program (Van Heuven, 2011). The dissociation constants of Goyet and Poisson (1989) were used due to their suitability at low temperatures (Brown et al., 2014). Here, pH is presented on the seawater scale (Goyet and Poisson, 1989).

Ice samples for DIC, TA and phosphate endmember values were collected between November and March 2014. Sea-ice samples were taken from cores of fast ice in Hangar Cove, north of Ryder Bay. Glacial samples were taken from the Sheldon Glacier (Fig. 1). Ice samples were sealed in Tedlar bags and air was removed using a hand pump. The samples were melted in the dark at lab temperature (18–20 °C) for 20–24 h and were then transferred to 250 mL borosilicate bottles, poisoned with mercuric chloride, sealed and stored in the dark until analysis. DIC and TA were measured at Rothera using a VINDTA 3C, as described above. Ice phosphate samples were drawn from the Tedlar bags, filtered (0.2 μM) and stored in the dark at −20 °C until analysis at the Royal Netherlands Institute for Sea Research. Seawater samples for oxygen isotope analysis were collected in 150 mL flat medical bottles, which were sealed with caps with rubber inserts, and parafilm to prevent slippage. They were transported to the UK via dark cool stow, for analysis by stable isotope mass spectrometry on an Isoprime spectrometer. Full details are provided in Meredith et al. (this issue).

The carbonate data presented here will be made available at the Carbon Dioxide Information Analysis Centre (CDIAC). Other RaTS time series data are available from Hugh Venables at the British Antarctic Survey.

2.2. Quantifying carbonate system processes

The processes affecting surface water DIC and TA at the study site were divided into four groups: the air–sea flux of CO_2; mixing of water masses; photosynthesis and respiration; the precipitation and dissolution of calcium carbonate. The rate of each of these process groups was quantified throughout the three year time series of carbon measurements using the approaches detailed in Sections 2.2.1–2.2.3. When calculating process rates, data were not binned or averaged; instead process rates were calculated using the change in measured variables from each discrete sampling time to the next in order to preserve as

much of the observed variability as possible. The time between discrete sampling times will be referred to as time steps.

A Monte Carlo approach was used to propagate uncertainty through our calculations, ensuring that all non-linearities in the carbonate system calculations were accounted for. Each calculation described below was carried out with 10^5 variable-value sets, randomly sampled from the statistical distributions of the variables, as described in the Appendix.

2.2.1. Air–sea CO_2 flux

Air–sea CO_2 flux was calculated as described in Legge et al. (2015), using gas transfer velocity calculated following Wanninkhof et al. (2013) and with a linear scaling to the fraction of open water, including all ice types. The daily calculated flux was divided by density and mixed layer depth to give the change to the mixed layer DIC concentration caused by air–sea flux. These daily values were summed over each time step and then divided by the length of the time step to give a process rate in units of μmol of DIC kg^{-1} d^{-1}. This estimate does not account for ice-atmosphere fluxes which we expect to be small compared to air–sea fluxes but may be significant over larger temporal and spatial scales (Delille et al., 2014).

2.2.2. Contribution of mixing

Water in Ryder Bay can be characterised as a mixture of three main sources: Circumpolar Deep Water (CDW), sea-ice melt and meteoric water (glacial melt and precipitation) (Meredith et al., 2008). This complexity means that a simple two endmember salinity normalisation of TA or DIC will fail to remove some of the variability caused in these variables by mixing. In order to capture the influence of the three water sources on DIC and TA we use measurements of salinity and oxygen isotopes ($\delta^{18}O$) to solve the following three endmember mass balance equations (Meredith et al., 2008, this issue):

$$f_{si} + f_{met} + f_{cdw} = 1$$
$$S_{si} \cdot f_{si} + S_{met} \cdot f_{met} + S_{cdw} \cdot f_{cdw} = S$$
$$\delta_{si} \cdot f_{si} + \delta_{met} \cdot f_{met} + \delta_{cdw} \cdot f_{cdw} = \delta \tag{1}$$

where f_{si}, f_{met} and f_{cdw} represent the fractions of sea-ice melt, meteoric water and CDW, respectively, which comprise the water sample in question. The salinity and $\delta^{18}O$ of the water sample are represented by S and δ respectively. S_{si}, S_{met} and S_{cdw} represent the salinity of the three endmembers and δ_{si}, δ_{met} and δ_{cdw} represent the $\delta^{18}O$ values of the three endmembers. Oxygen isotope and salinity samples were taken at the same time and location as the carbonate chemistry samples so the percentage contributions calculated here directly correspond to the DIC and TA data points in time and space.

To quantify the change in DIC and TA due to mixing during each time step, the change in the percentage contribution of each endmember over that time step was multiplied by its concentration of DIC and TA (Eq. (2)). The endmember concentrations used for salinity, $\delta^{18}O$, DIC and TA in CDW, sea-ice melt and meteoric water are detailed in the Appendix.

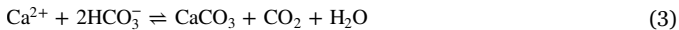$$\Delta DIC_{mix} = \Delta CDW \cdot [DIC]_{cdw} + \Delta MET \cdot [DIC]_{met} + \Delta SI \cdot [DIC]_{si} \tag{2}$$

where ΔDIC_{mix} is the change in DIC due to mixing over a given time step, ΔCDW, ΔMET and ΔSI are the changes in fractional contributions of the three water sources over the time step and $[DIC]_{cdw}$, $[DIC]_{met}$ and $[DIC]_{si}$ are the DIC concentrations of the three endmembers. The same method was used for TA. The change in DIC due to mixing over each time step was divided by the length of the time step to give a process rate in units of μmol kg^{-1} d^{-1}.

2.2.3. Quantifying net dissolution and net respiration

Once the effects of mixing and air–sea flux have been removed, any remaining change observed in DIC and TA over a time step must come from the balance of precipitation and dissolution of calcium carbonate and from the balance of photosynthesis and respiration. These processes were quantified simultaneously using their known effects

on the relative concentrations of DIC and TA. We believe that the method detailed below is novel and is a useful tool when quantifying carbonate system processes as it explicitly quantifies the precipitation and dissolution of calcium carbonate rather than leaving these processes as a residual.

The formation and dissolution of calcium carbonate changes TA and DIC in a 2:1 ratio (Zeebe and Wolf-Gladrow, 2001) as one mole of DIC and two negative charge equivalents are consumed to produce one mole of calcium carbonate:

$$Ca^{2+} + 2HCO_3^- \rightleftharpoons CaCO_3 + CO_2 + H_2O \qquad (3)$$

Photosynthesis reduces the concentration of DIC in the water as it is incorporated into organic matter and the reverse is true for respiration. Photosynthesis and respiration do not have a direct effect on carbonate alkalinity although they do cause a slight TA increase and decrease, respectively, due to the assimilation and remineralisation of nutrients (Brewer and Goldman, 1976). When phytoplankton take up nitrate they also take up protons thereby increasing alkalinity. The ratio of the influence of photosynthesis and respiration on DIC and TA therefore depends on the carbon to nitrogen ratio of the organic matter being produced or respired. This ratio can be approximated as 106:16 (Redfield et al., 1963) but varies depending on the evolutionary history of the primary producer, growth rate and nutrient availability (Geider and La Roche, 2002; Quigg et al., 2003; Arrigo, 2005). We have attempted to account for this variability in our uncertainty analysis (see distributions in the Appendix). For the sake of brevity we will refer to the balance of calcium carbonate precipitation and dissolution as net dissolution because a positive rate indicates increasing DIC through net dissolution. Similarly, the balance of photosynthesis and respiration will be referred to as net respiration.

For each time step, the change in DIC and TA due to net respiration and net dissolution was calculated by using the known slopes of these processes in DIC/TA space (green and cyan coloured lines, Fig. 2). The DIC and TA values at the intersection of these process slopes were calculated using Eqs. (4) and (5). This intersection allows the calculation of the change in both DIC and TA caused by each process. The change in DIC due to net respiration and the change in DIC due to net dissolution were then divided by the length of the time step to give rates for these processes in units of $\mu mol\,kg^{-1}\,d^{-1}$. The graphical example in Fig. 2 highlights the Monte Carlo approach whereby the process rates for each time step were calculated 10^5 times to incorporate various uncertainties (see Appendix):

$$DIC_i = \frac{(TA_2 - M_{diss}. DIC_2) - (TA_1 - M_{resp}. DIC_1)}{M_{resp} - M_{diss}} \qquad (4)$$

$$TA_i = M_{resp}. (DIC_i - DIC_1) + TA_1 \qquad (5)$$

where i denotes the DIC or TA at the intersection between the two process slopes (the point where green and cyan lines meet in Fig. 2), M_{resp} is the slope of photosynthesis and respiration in DIC/TA space and M_{diss} is the slope of precipitation and dissolution of calcium carbonate in DIC/TA space. The subscript $_1$ denotes the DIC or TA concentration at the start of the time step, after the effects of mixing and air–sea CO_2 flux have been accounted for. The subscript $_2$ denotes the DIC or TA concentration at the end of the time step.

2.2.4. Quantifying net respiration from phosphate

Phosphate data were used to obtain an estimate of net respiration, independently from the carbon measurements. Firstly, the effect of mixing on phosphate concentration over each time step was calculated using the endmember approach described above for DIC and TA. The endmember values of phosphate in CDW, sea ice and meteoric water are detailed in the Appendix. It should be noted that inaccuracies in the percentage contribution of the three endmember water masses affects both carbon and phosphate-derived net respiration estimates. Once the effect of mixing was removed from the measured changes, the remain-
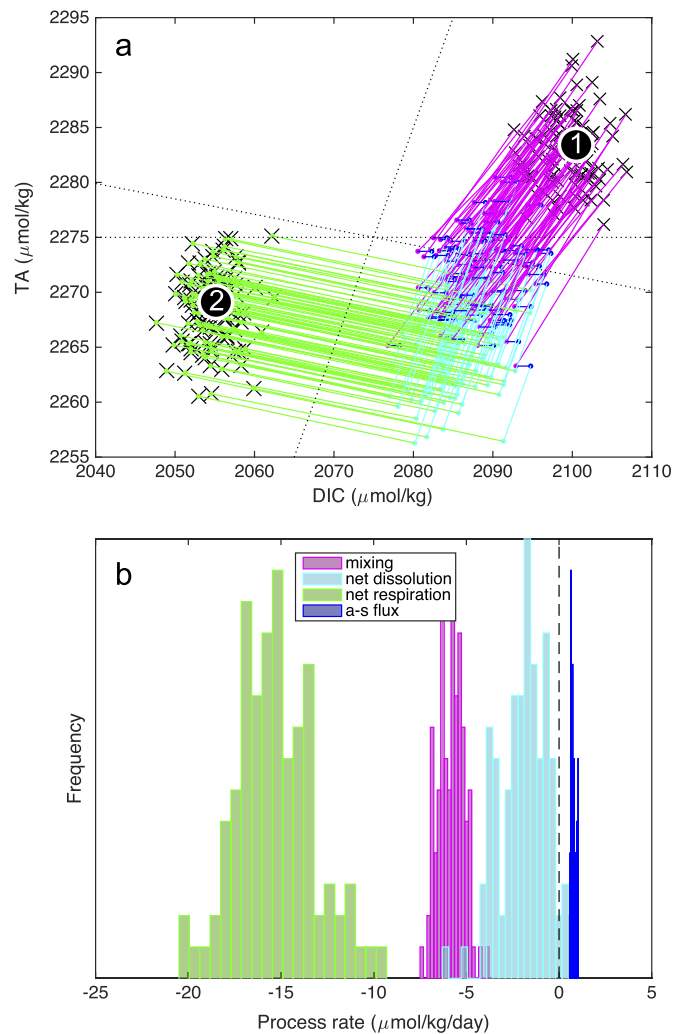
Fig. 2. A graphical example of process rate calculations in DIC/TA space for one time step. (a) The paths taken through DIC/TA space by a random subset of the Monte Carlo runs for this time step. A subset is used for visual clarity. The points marked '1' and '2' show the measured DIC and TA at the start (19th January 2013) and end (21st January 2013) of the time step respectively. Crosses represent the DIC and TA values used in the Monte Carlo analysis for the start and end of the time step and their spread represents the uncertainty on DIC and TA measurements. Pink lines represent the change in DIC and TA due to mixing, dark blue lines represent the change in DIC and TA due to air–sea CO_2 flux, cyan lines represent the change in DIC and TA due to the precipitation and dissolution of calcium carbonate and green lines represent the change in DIC and TA due to photosynthesis and respiration. See the appendix for a description of the uncertainties used in the Monte Carlo analysis. (b) Probability distributions for the processes affecting DIC during this time step. The same subset of Monte Carlo runs is shown as in panel a.

ing change in phosphate concentrations over each time step was multiplied by the ratio of phosphorus to carbon in organic matter. Variability in the elemental ratios of organic matter has been accounted for in our Monte Carlo approach and is discussed in the Appendix.

2.3. Method limitations

The method used here to quantify water mass contributions gives a good first order estimate of the effect of mixing on the carbonate system. However, it does not resolve some physical processes influencing DIC and TA in Ryder Bay and these inaccuracies may affect the calculated rates of net respiration and net dissolution. Firstly, using water mass contributions based on the conservative tracers salinity and $\delta^{18}O$ will not capture changes caused by advection in the Bay and may cause the rate of biogeochemical processes to be over- or under-estimated. This limitation is probably responsible for much of the

short-term variability in the calculated net respiration and net dissolution rates because, although we expect the surface water in the whole bay to follow broadly the same seasonal pattern, there is likely to be significant horizontal variability in primary production and mixing over shorter spatial and temporal scales. Monthly and seasonal averages of process rates should therefore provide more representative rate estimates for the bay as a whole. Secondly, the endmember method used here calculates the net change in the percentage contribution of each water mass over each time step, but it is likely that during a time step there are gross changes which are not captured by this method and which deliver carbon or nutrients to the sampling depth. If some of these chemicals are taken up and retained in the surface water, then the change will be attributed to biogeochemical processes and the mixing term will be underestimated. Finally, characterising CDW as one homogeneous endmember is an over-simplification. In reality there are vertical gradients of DIC, TA and nutrients in the water column and, due to biogeochemical processes, these gradients are unlikely to be conservative with the calculated percentage of CDW. More data on the vertical and horizontal variability of DIC, TA and nutrients would allow a more sophisticated calculation of mixing.

It is important to note that, when calculating net dissolution and net respiration from surface DIC and TA concentrations (Section 2.2.3), the signal of these processes within sea ice will also be captured. However, there may be some time delay in our process rate estimates as any ice-derived signal is not measured until the ice melts or brine is released into the underlying water.

A caveat to the air–sea flux calculations is that during the summer the water column can be highly stratified with a mixed layer shallower than our 15 m sampling depth (Fig. 3). The water fCO$_2$ used in the flux calculations may therefore not be representative of the fCO$_2$ in contact with the atmosphere. We expect that this results in an underestimation of the ocean uptake of atmospheric CO$_2$ because surface water is likely to have lower fCO$_2$ than our sampling depth due to ice melt and photosynthesis.

3. Results

3.1. The observed carbonate system

Both DIC and TA data exhibit a strong, asymmetric seasonal cycle (Fig. 4). Their concentrations increase gradually during the autumn and winter to maximum values of ~2200 µmol kg^{-1} of DIC and ~2295 µmol kg^{-1} of TA in September. The rapid decrease in DIC and TA in December and January is preceded by a more gradual decrease during October and November. An interesting feature which recurs in each of the three years sampled is a rapid, short-lived decrease in TA in March of about 30 µmol kg^{-1} relative to surrounding values.

The fugacity of CO$_2$ in water largely follows the seasonal pattern of DIC and has an amplitude of ~300 µatm (Fig. 5). The fCO$_2$ of the water is greater than in the overlying atmosphere in winter and lower in the summer, leading to a change in the direction of the air–sea flux of CO$_2$, with the ocean being a net sink of atmospheric CO$_2$ in summer and a net source in winter (Legge et al., 2015). The pH and the saturation states of the calcium carbonate minerals calcite and aragonite show a rapid increase in December /January followed by a more gradual and variable decrease to a winter minimum (Fig. 5). The pH ranges from ~7.95 to ~8.4. The saturation state of calcite ranges from ~1.5 to ~4.5 whereas the more soluble calcium carbonate polymorph, aragonite, has saturation states ranging from ~1.0 to ~2.8.

Carbonate system data from the two RaTS sampling sites generally agree well. During the winter months, when the water column is well mixed, DIC and TA data from the two sampling depths agree closely but as the water column stratifies in spring and summer the 15 m values decrease more rapidly than those from 40 m, due to primary production in the surface layer and the persistent influence of CDW at depth. Although the seasonal cycle of the carbonate system variables is broadly consistent between the three observed years, there is intriguing
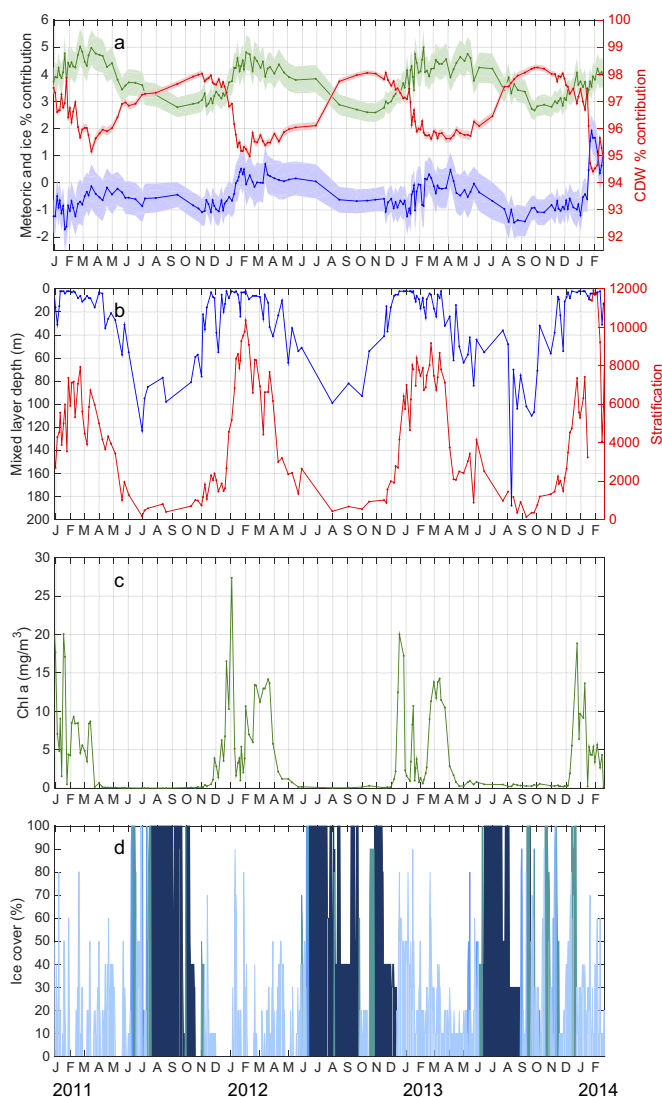

Fig. 3. Factors influencing the carbonate system in Ryder Bay. (a) Percentage contribution of meteoric water (green), sea ice (blue) and CDW (red) to the water at 15 m; (b) Mixed layer depth (blue) and stratification (red). Stratification is expressed as the energy in J/m^2 required to homogenise the top 100 m; (c) Chlorophyll-a concentration at 15 m depth; (d) Percentage ice cover. Bar colour denotes ice type. Dark blue represents fast ice, turquoise represents pack ice and light blue represents brash ice.

interannual variability. The DIC and water fCO$_2$ is greater in winter 2013 than in the two preceding years (Legge et al., 2015) and there is a corresponding decrease in winter pH and calcium carbonate saturation states. The exact timing and magnitude of the main, summer DIC drawdown is not identical between the four years and the TA appears to behave slightly differently in each of these productive periods. At the very start of the time series in December 2010/ January 2011 there are unseasonably low TA values compared to the other years, leading to low pH and calcium carbonate saturation states.

3.2. Processes

The method presented here allows us to quantify the seasonal cycle of the four processes affecting the carbonate system and to determine their relative importance during the year. Fig. 6 shows the process rates calculated for each measured time step. All process rates are greatest between November and March and are very low in winter. There is very large variability in process rates, especially net respiration which ranges from −35 to 25 µmol kg^{-1} d^{-1} during the productive summer season.

Monthly and seasonal averages of process rates (Figs. 7 and 8)
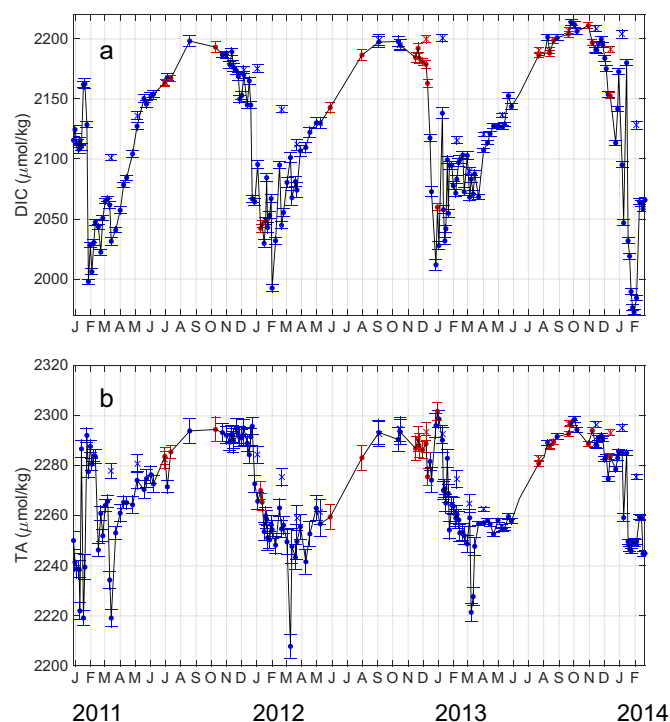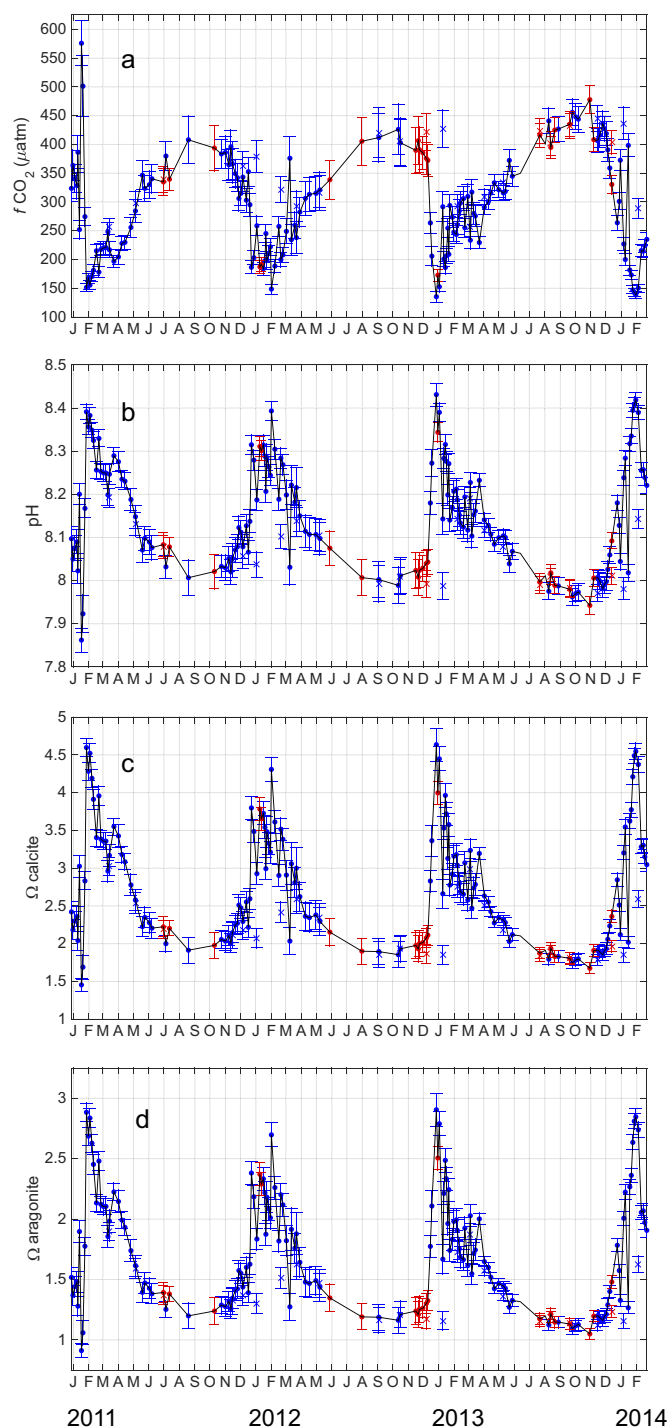
Fig. 4. Measured carbonate system variables. (a) Dissolved inorganic carbon, (b) total alkalinity. Dots represent data from 15 m, crosses represent data from 40 m. Blue points are from RaTS site 1 and red points are from site 2. Error bars represent approximate 95% confidence based on measurement precision. DIC panel after Legge et al. (2015). (For interpretation of the references to colour in this figure caption, the reader is referred to the web version of this paper.)

present the seasonal cycle more clearly and average out some of the shorter time scale variability, which is likely caused by advection (see Section 2.3). Mixing reduces the DIC concentration between October and March and increases the DIC concentration from April to September. The largest change due to mixing is in January, although there is significant interannual variability between the four observed years (Fig. 7). The results of the salinity and $\delta^{18}O$ method to determine water mass contributions are shown in Fig. 3 and are investigated thoroughly by Meredith et al. (this issue). The water in Ryder Bay is dominated by CDW (95–98%). Meteoric and sea-ice components decrease in the austral winter and increase in the austral summer with meteoric contributions being consistently greater than sea-ice contributions. Negative sea-ice contributions indicate that there has been a net sea-ice production from that water prior to it being sampled. Percentage contributions of sea ice do not coincide directly with ice observer estimates of ice cover due to different advection of ice and water into and out of Ryder Bay (Meredith et al., 2008).

The strong seasonal cycle of air–sea CO_2 flux increases the surface ocean DIC concentration in summer and reduces it in winter, and in all three years the summer uptake exceeds the winter out-gassing (Fig. 7). This seasonal asymmetry is accentuated when the air–sea flux is expressed in $\mu mol\,kg^{-1}\,d^{-1}$ for the mixed layer because the mixed layer depth is greatest in winter, making the change to the DIC concentration smaller for a given flux of CO_2 across the water–air interface. There is considerable interannual variability in the monthly mean flux rates. In 2013, air–sea fluxes were lower than average in both summer and winter (Figs. 7 and 8), resulting in a weaker net ocean sink of atmospheric CO_2 in 2013 than in the previous two years.

Primary production also shows a clear seasonal cycle with net respiration increasing DIC concentrations during the winter months and net photosynthesis reducing DIC in summer (Fig. 7). Net photosynthesis is consistently highest in December and January although there is large interannual variability in the magnitude of the monthly

Fig. 5. Calculated carbonate system variables. (a) fCO_2, (b) pH, (c) calcite saturation state and (d) aragonite saturation state. Dots represent data from 15 m, crosses represent data from 40 m. Blue points are from RaTS site 1 and red points are from site 2. Error bars represent approximate 95% confidence based on measurement precision and dissociation constants. (For interpretation of the references to colour in this figure caption, the reader is referred to the web version of this paper.)

means in these months. The monthly averaged rates of net calcium carbonate dissolution (Fig. 7) are low (less than $0.15\,\mu mol\,kg^{-1}\,d^{-1}$) and in only one month do all year's monthly means agree on the sign of the process, making identification of a seasonal pattern impossible.
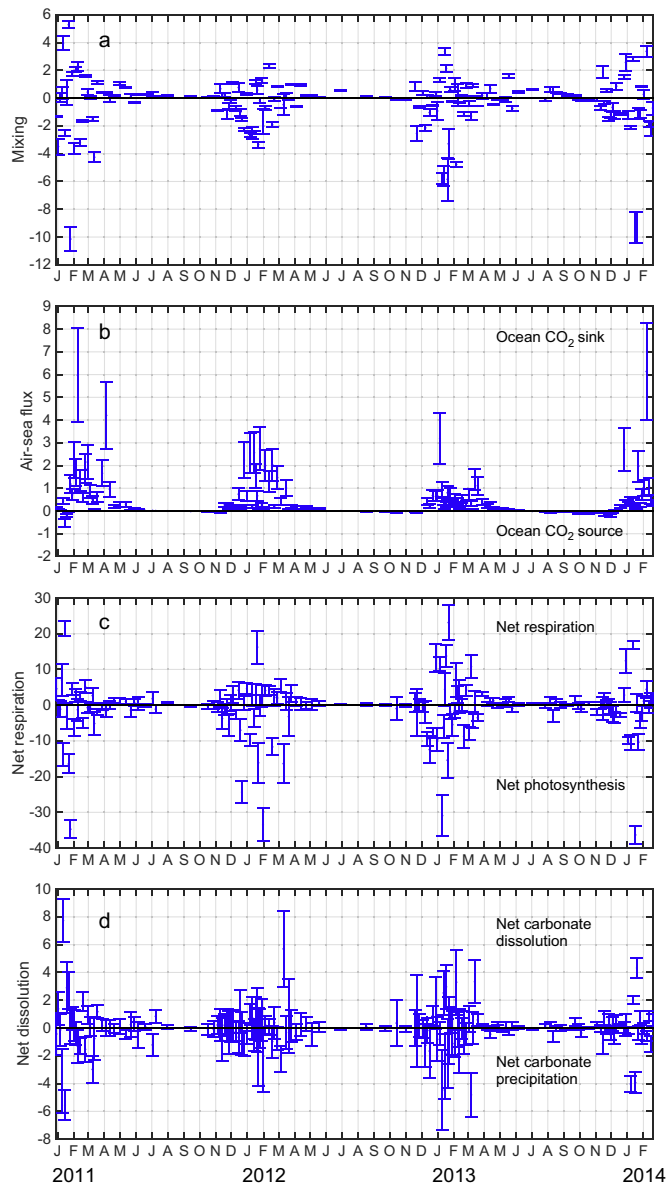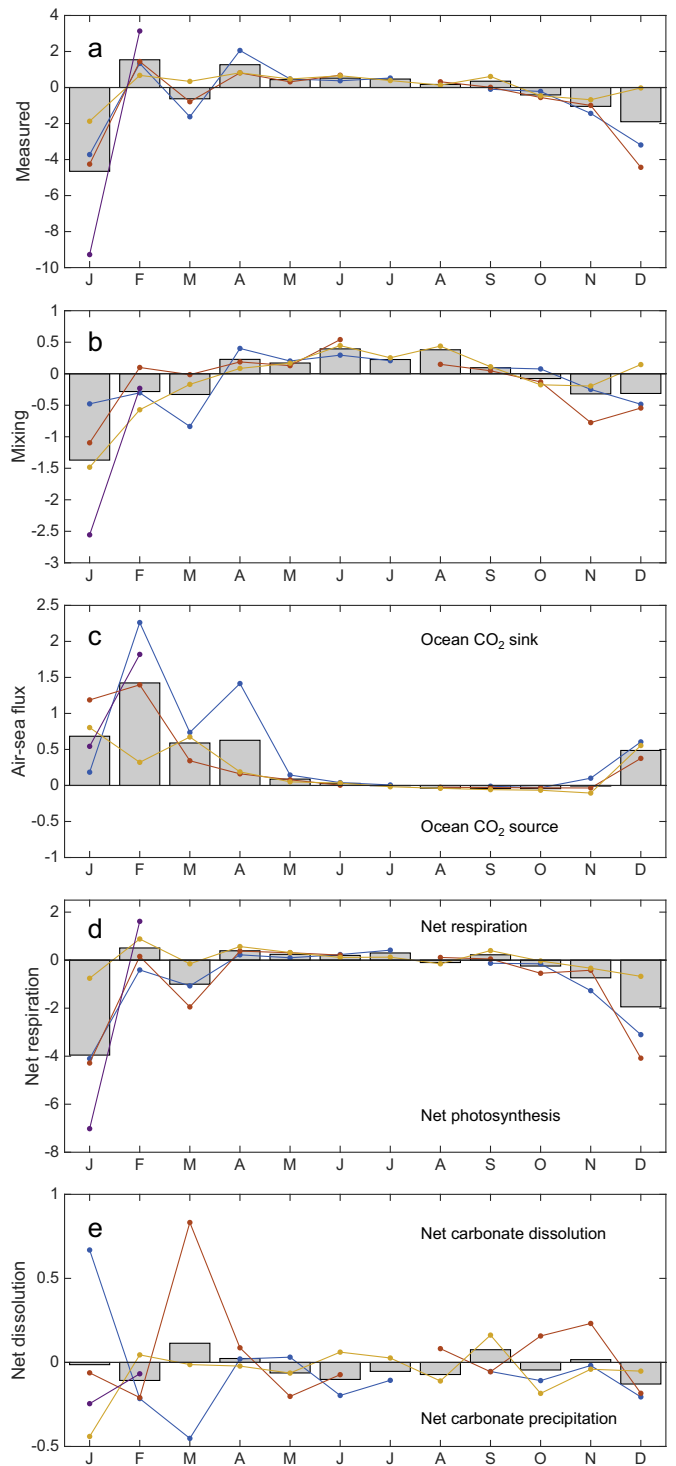
Fig. 6. Calculated rates of processes affecting DIC in the surface water of Ryder Bay, expressed in μmol DIC kg^{-1} d^{-1}. (a) Mixing, (b) air–sea CO_2 flux, (c) net respiration and (d) net dissolution. Error bars represent approximate 95% confidence from Monte Carlo analysis.

## 4. Discussion

4.1. Saturation states

The seasonal cycle of Ω aragonite presented here is very similar in timing and amplitude to that observed in the coastal Ross Sea (Sweeney, 2003; McNeil et al., 2011) although the Ross Sea study lacked winter data. Comparison with Prydz Bay in East Antarctica is more challenging as the two seasonal cycles of pH and Ω observed there in 1993–1995 (Gibson and Trull, 1999; McNeil et al., 2011) and 2010–2011 (Roden et al., 2013) are quite different in timing and amplitude. Our Ω data show a similar pattern to the more recent Prydz Bay data (2010–2011) although Ω in Ryder Bay reaches much higher values; Ω aragonite in Prydz Bay did not exceed 2 during summer 2010–2011 (Roden et al., 2013). Our results broadly corroborate the estimates of Hauri et al. (2015) who used pCO$_2$, salinity and temperature data from the Pal-LTER grid to calculate aragonite saturation state for the waters of the WAP shelf between 1999 and 2013. They found

Fig. 7. Monthly mean rates of processes affecting DIC in the surface water of Ryder Bay. (a) Measured rate of change of DIC, (b) mixing, (c) air–sea CO_2 flux, (d) net respiration, (e) net dissolution. All rates are expressed in units of μmol DIC kg^{-1} d^{-1}. Grey bars are the monthly averages including data from all years of carbon sampling. Coloured points represent monthly means of individual years (blue: 2011, red: 2012, yellow: 2013, purple: 2014). Note the different scale for different processes. (For interpretation of the references to colour in this figure caption, the reader is referred to the web version of this paper.)

large interannual variability and more than 20% of their calculated winter and spring values fell below 1.2.

Some Arctic studies have found that melting ice can lower Ω through dilution of carbonate ions in the water (Chierici and Fransson, 2009; Yamamoto-Kawai et al., 2009). However, consistent
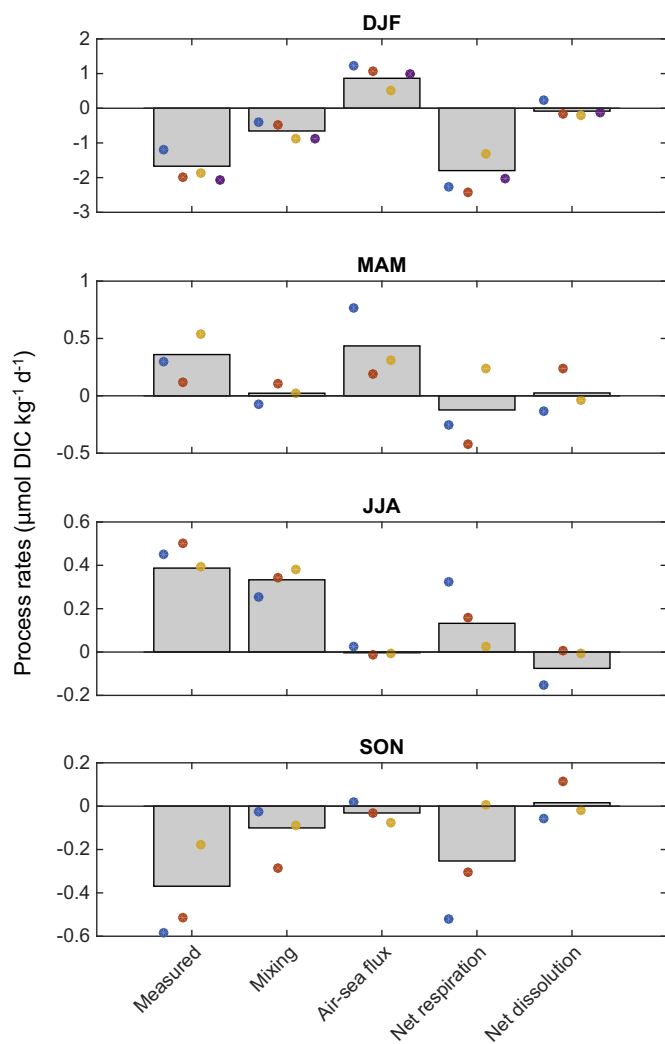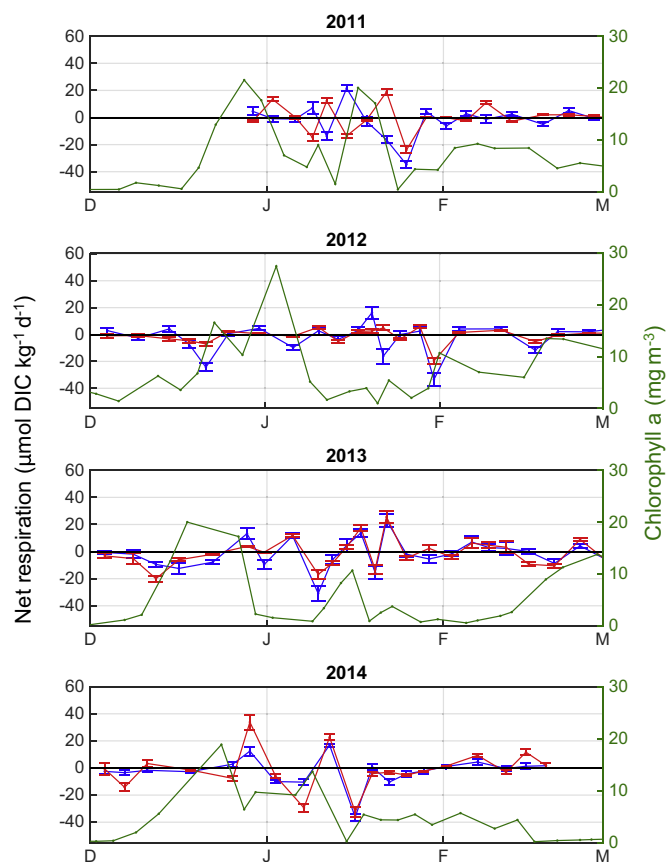
Fig. 8. Seasonal mean rates of processes affecting DIC in the surface water of Ryder Bay. Grey bars represent the seasonal mean process rates from all years of carbon sampling. Dots represent seasonal means from individual years of the time series (blue: 2011, red: 2012, yellow: 2013, purple: 2014). All rates are expressed in units of μmol DIC kg⁻¹ d⁻¹. The seasonal means have be calculated as the mean of the three monthly means in each season (DJF, MAM, JJA and SON) to avoid sampling bias. Note different scale for different seasons. (For interpretation of the references to colour in this figure caption, the reader is referred to the web version of this paper.)

Fig. 9. Carbon (blue) and phosphate (red) derived net respiration rates during the four summer seasons. Rates > 0 indicate net respiration and rates < 0 indicate net photosynthesis. Error bars represent uncertainty from Monte Carlo analysis. Chlorophyll-a concentration at 15 m is shown in green.

with other Southern Ocean studies (Mattsdotter Björk et al., 2014; Shadwick et al., 2013), we find that increasing percentage contributions of glacial and sea-ice melt in summer coincide with increasing Ω, suggesting that DIC uptake by primary production outweighs any dilution effect. We note, however, that our sampling depth is at the typical chlorophyll maximum in Ryder Bay (Clarke et al., 2008) and the dilution effect of melt water on pH and Ω in the highly stratified water above may be more significant relative to primary production.

4.2. The seasonal cycle of carbonate processes

4.2.1. Summer (December, January, February)

The dominant carbonate system process in summer (December, January and February) is primary production; the reduction in DIC caused by photosynthesis is roughly twice as large as the reduction in DIC due to mixing (Fig. 8). In all years the highest rates of photosynthesis are in December and January, coincident with the main phytoplankton bloom and rapidly increasing stratification (Fig. 3) and the main periods of net photosynthesis broadly correspond to increasing chlorophyll concentrations (Fig. 9). The interannual varia-

bility in the magnitude of net photosynthesis in December and January (Fig. 7) is largely caused by slight differences in the timing of the main bloom between years and is consistent with earlier observations of significant interannual variability in the intensity, timing and depth of blooms in Ryder Bay (Clarke et al., 2008). The summer seasonal averages for the four years are more similar, showing that, when process rates are averaged over the whole growing season, there is less variability between years.

Ice melt, warming and a reduction in wind speed cause stratification of the water column in summer (Meredith et al., 2004, 2010) which restricts mixing of deeper, carbon-rich water into the mixed layer. The increase in ice melt and decrease in CDW is greatest in January (Fig. 3) resulting in a strong reduction in DIC (Fig. 7). Particularly high percentage contributions of sea-ice melt and low contributions of CDW are observed in January 2014 which results in a larger reduction in DIC than in previous years. Here, the influence of sea-ice melt on the carbonate system is accentuated because several weeks of ice melt signal are integrated into one mixing event; stratification and mixed layer depth during December 2013 and early January 2014 indicate a shallow, stable surface layer (Fig. 3) and it is the effect of this fresher, low DIC water that we observe in mid-January as it is mixed to our sampling depth. This period therefore serves as a useful example of how ice melt reduces surface ocean DIC concentration in Ryder Bay during summer.

Alkalinity data show a sudden and short-lived increase at the end of December 2012, at the end of the main DIC drawdown, and a similar pattern occurs at the end of January/ start of February 2011 (Fig. 4). During both of these periods the mixed layer is very shallow and sea-ice cover is decreasing. In both cases, concurrent with the increase in TA, water temperature at 15 m increases by at least 1 °C (see temperature

plot in Appendix) and we speculate that the observed alkalinity increase may be caused by dissolution of the calcium carbonate mineral ikaite ($CaCO_3.6H_2O$) as it is released from overlying, melting ice (Rysgaard et al., 2007, 2011; Dieckmann et al., 2008; Fransson et al., 2013).

At the start of the time series, in January 2011, the measured TA is highly variable, reaching values roughly 30 μmol kg^{-1} lower than the same period in the following three years (Fig. 4). This causes unusually low pH and Ω (Fig. 5). A large decrease in TA relative to DIC suggests the precipitation of calcium carbonate, either by biological calcification or the formation of ikaite in ice, but the observed changes are probably too sudden to be purely biogeochemical and we expect this variability to also be caused by advection. Both advection and biogeochemical processes are influenced by larger scale physical forcings and we speculate that the unusual behaviour of the carbonate system in January 2011 may be related to wind forcing. The percentage ice cover in the winter preceding these low TA values was lower than in the three subsequent winters and the percentage contribution to the water from sea ice was more negative, suggesting that a greater area of exposed water led to more heat loss and more ice formation and subsequent ice export (Meredith et al., 2010). The winds during the ice season of 2010 were stronger and more northerly than during the three subsequent years (wind roses are shown in the Appendix), allowing more ice to be produced and exported from the southward facing Ryder Bay in late 2010. This observed interannual variability in wind strength and direction is likely related to the large scale atmospheric changes driven by the Southern Annular Mode (SAM) and the El Niño Southern Oscillation (ENSO) which had strong positive and negative anomalies, respectively, in 2010.

Some of the observed carbonate system variability at the start of the time series may also be related to vertical mixing. The percentage contribution of CDW at our sampling depth is higher and more variable during January 2011 than during the following three Januaries and salinity profiles indicate higher salinity water reaching shallower in the water column. This is likely caused by increased mixing due to stronger northerlies and the related low ice cover. The data presented here do not provide sufficient spatial or temporal resolution to resolve a mechanistic connection between interannual variability in wind and ice cover, and alkalinity.

4.2.2. Autumn (March, April, May)

On average, the dominant carbonate system process in autumn (March, April and May) is air–sea flux which increases the DIC concentration (Fig. 8). Although the rate of DIC change due to air–sea flux is often smaller than that due to mixing or net respiration over short timescales (Fig. 6), its influence on a monthly or seasonal scale is large because it consistently acts in one direction during this period. The ocean uptake of CO_2 in autumn is greater in 2011 than the two following years due to the lower water fCO$_2$ in April 2011 (Fig. 5). In all years sampled there is an increase in net respiration from January to February and a decrease from February to March (Fig. 7). This pattern reflects the chlorophyll-a climatology which suggests a late season chlorophyll peak in March, separate from the initial summer bloom (Clarke et al., 2008).

The rapid decrease in TA in March in all three years sampled (Fig. 4) appears to be caused by significant precipitation of calcium carbonate, quickly followed by dissolution although the mechanism behind this recurring signal remains unclear. This may be caused by calcifying organisms although we have no information of significant numbers of calcifiers in Ryder Bay. Alternatively, this signal could originate from sea-ice processes although in all three years the bay had been free of pack and fast ice for at least two months by early March.

4.2.3. Winter (June, July and August)

In winter (June, July and August), the deepening mixed layer increases the percentage contribution of CDW, resulting in an increase

in DIC. Ice formation, as evidenced by negative percentage contribution of sea ice (Fig. 3), also increases the DIC and CO_2 concentrations of the underlying water due to brine rejection, causing a decrease in the saturation state of calcium carbonate minerals (Rysgaard et al., 2007; Chierici et al., 2011; Miller et al., 2011; Shadwick et al., 2011; Fransson et al., 2013). We find mixing to be the dominant influence on the carbonate system in winter. Day length, temperature and ice cover limit primary production during the winter and the surface water in Ryder Bay is slightly net heterotrophic from April to September (Fig. 7), although there is considerable interannual variability in the magnitude of this net respiration.

4.2.4. Spring (September, October and November)

The rapid drawdown of DIC in December and January is preceded by a more gradual DIC decrease in November and we find net photosynthesis in November in all three years (Fig. 7). The chlorophyll concentration at 15 m during October and November is very low (Fig. 3) and it is possible that some of this early season photosynthesis signal comes from ice algae which make a significant contribution to primary production in the Antarctic (Arrigo et al., 2009), especially in early spring and late summer (Meiners et al., 2012). The relative timing of primary production and ice melt have the potential to greatly affect the air–sea CO_2 flux and thereby the strength of the ocean carbon sink. Studies in the Ross Sea (Sweeney, 2003), Prydz Bay (Gibson and Trull, 1999; Roden et al., 2013), the Weddell gyre (Bakker et al., 2008) and the Weddell-Scotia confluence (Jones et al., 2010) found a significant decrease in water fCO$_2$ due to primary production prior to complete ice melt, creating a sink for atmospheric CO_2. In Ryder Bay, during the three years presented here, the ice season was shorter than that observed by the above studies and we find the majority of fCO$_2$ drawdown to occur in the main bloom period in December and January, after most fast and pack ice have melted. There is a significant fraction of open water in Ryder Bay for a period of weeks or months prior to the rapid increase in chlorophyll (Fig. 3). In all three spring periods the reduction of fCO$_2$ in October and November, prior to the main chlorophyll increase, is insufficient to make the water fCO$_2$ lower than that of the atmosphere so the ocean remains a source of CO_2 to the atmosphere until the main bloom.

Meltwater from sea ice and glacial ice reduces surface water DIC and fCO$_2$ in spring, prior to the main phytoplankton bloom. Meltwater therefore influences the air–sea flux of CO_2 (Rysgaard et al., 2011) and contributes to the net annual ocean sink for atmospheric CO_2 in Ryder Bay (Legge et al., 2015). The percentage contribution of meteoric water to the bay is greater than that of sea ice (Fig. 3a) and its seasonal amplitude is also slightly greater, making glacial meltwater more influential than sea-ice melt in terms of its direct impact on carbonate chemistry in Ryder Bay.

The DIC reached higher values during September and October 2013 than in the two previous years (Fig. 4) causing higher surface water fCO$_2$ which, combined with a reduction in ice cover, leads to an increase in the calculated flux of CO_2 from the ocean to the atmosphere (Legge et al., 2015). We suggest that the higher DIC values in 2013 are caused by increased mixing of carbon-rich CDW to the surface; this is supported by the higher percentage contribution of CDW (Fig. 3) and by the observation that higher salinity water reaches shallower in the water column (see salinity plot in the Appendix). A reduction in ice melt could also lead to higher surface water DIC due to a reduction in dilution and stratification. The higher DIC concentration during September and October 2013 also leads to lower pH and calcium carbonate saturation states than in the two previous years (Fig. 5) and brings Ω aragonite very close to 1. These observations suggest that future changes to the delivery of CDW to the surface ocean may significantly affect carbonate chemistry in the surface ocean with implications for the ocean sink of atmospheric CO_2 and the life cycle of calcifying organisms.

4.3. Comparison of carbon and phosphate derived net respiration

A comparison of the net respiration rates in summer derived from carbonate system calculations and those calculated from phosphate gives mixed results (Fig. 9). Carbon and phosphate estimates agree well both in direction and magnitude during the summer of 2013 and show broad agreement during the summers of 2012 and 2014. In 2011 however, the two methods agree less well, disagreeing on the sign of the process for much of January. We expect that much of the disagreement between the carbon and phosphate methods may be related to mixing and it is worth noting that inaccuracies in the mixing term (Section 2.3) may affect phosphate more than DIC because surface phosphate values show a greater range relative to their deep concentrations than DIC. On average, the carbon based estimate of photosynthesis exceeds the nutrient based estimate. This pattern is not uncommon (Laws, 1991; Sambrotto et al., 1993; Brzezinski et al., 2003; Green and Sambrotto, 2006) and has been attributed to preferential recycling of limiting nutrients (Thomas et al., 1999; Bozec et al., 2006). However, we expect that, overall, nutrient utilisation at RaTS is close to Redfieldian (Clarke et al., 2008) and that much of the difference is caused by inaccuracies in our mixing term. With carbonate and phosphate data predominantly from one sampling depth we are unable to resolve the net community production over the full depth of the water column during our study period. Vertical profile data, especially during the summer season would allow a vertically integrated measure of primary production using a carbon and nutrient deficit approach (Hoppema et al., 2002; Shadwick et al., 2011; Weston et al., 2013; Jones et al., this issue).

5. Conclusions

We observe a strong seasonal cycle in the carbonate system in the surface water of Ryder Bay driven by physical and biological processes. In winter, mixing with deeper water increases the DIC concentration at the surface whereas in spring and summer, stratification and ice melt from glaciers and sea ice reduce DIC. Air–sea CO_2 flux increases DIC in the water in summer and autumn and reduces it in winter and spring.

The dominant process affecting DIC in summer is primary production, however, we expect that the consumption of DIC in summer by primary production in Ryder Bay is higher than would be found farther offshore due to near-shore glacial influence on stratification and nutrient delivery. Marguerite Bay, adjoining Ryder Bay, has persistently higher chlorophyll concentrations than other areas of the WAP (Marrari et al., 2008) and summer studies have found higher oxygen saturations, lower CO_2 saturations and higher net community production in Marguerite Bay than on the rest of the WAP shelf (Carrillo et al., 2004; Tortell et al., 2015), suggesting that the net respiration and air–sea CO_2 flux rates shown here are not scalable to the WAP shelf as a whole.

Appendix A. Distribution of variables

In order to perform the Monte Carlo analysis, each value of each variable was given a distribution to represent its uncertainty and this distribution was randomly sampled 10^5 times. DIC and TA were given normal distributions with the population mean being the measured value and the uncertainty defined using replicate precision specific to each of the three field seasons. The reason for using different uncertainty estimates for different field seasons is that, although instrument precision remains fairly stable between different years (long term standard deviation of certified reference material of 2.2 μmol kg^{-1} or less for both DIC and TA), there is considerable variation in replicate precision between different field seasons. This could reflect differences in sampling, poisoning, storage and transport. The DIC and TA standard deviations in 2010–2012 were 4.3 μmol kg^{-1} and 4.9 μmol kg^{-1} respectively. In 2012–2013 they were 6.2 μmol kg^{-1} and 7.0 μmol kg^{-1} and in 2013–2014 they were 3.4 μmol kg^{-1} and 1.5 μmol kg^{-1}. The uncertainty used here for a given DIC or TA value is the replicate precision of the relevant field season divided by the square root of the number of replicates from that time and location.

Phosphate was given normal distributions with the population mean being the measured value and the uncertainty defined as precision determined by the analyst (2.7%). The dissociation constants of Goyet and Poisson (1989) were used in CO2SYS and were given normal distributions with uncertainties of 0.0055 for pK1 and 0.01 for pK2 (Millero, 2007). The sum of the air–sea CO_2 flux during each time step was given a uniform distribution of 30% either side of the calculated value to account for the high degree of uncertainty associated with this process. In

Table 1

Distributions of endmember variables. Distributions with ± are normal and have been truncated at zero. Distributions with a range are uniform. Salinity and $\delta^{18}O$ endmembers are based on Meredith et al. (2008). CDW DIC and TA endmembers are based on Hauri et al. (2015). The CDW phosphate endmember is based on Henley et al. (this issue). Sea ice and glacial ice DIC, TA and phosphate endmembers are from ice samples collected close to the study site (see methods).

Variable	CDW	Meteoric	Sea ice
Salinity	34.62 ± 0.01	0	7 ± 1
$\delta^{18}O$ (‰)	0.08 ± 0.01	−22 to −13	1.8–2.7
DIC (μmol kg^{-1})	2253 ± 20	16 ± 5	277 ± 150
TA (μmol kg^{-1})	2350 ± 20	100 ± 5	328 ± 150
Phosphate (μmol kg^{-1})	2.2–2.6	0–0.03	0.5 ± 0.7

order to account for uncertainties in the endmember approach used to quantify mixing processes, each endmember was given distributions for salinity, $\delta^{18}O$, DIC, TA and phosphate (Table 1). Most of the uncertainty in the $\delta^{18}O$/salinity method to quantify water mass contributions comes from the value of the $\delta^{18}O$ and salinity endmembers. This is largely a systematic uncertainty and therefore cancels out when the change over a time step is calculated.

The relative influence on DIC and TA by photosynthesis and respiration is determined by the carbon to nitrogen ratio of primary producers (see Section 2.2.3). Studies in the region find the C:N ratio to be close to Redfieldian (Rubin et al., 1998; Martiny et al., 2013; Hauri et al., 2015) so we have assigned the C:N ratio a normal distribution with a mean of 6.6 and a standard deviation of 0.25. Clarke et al. (2008) found an average nitrate to phosphate ratio of 15.3 in Ryder Bay. When using phosphate data to calculate net respiration in Section 2.2.4 we therefore use the C:N distribution described above, multiplied by 15.3.
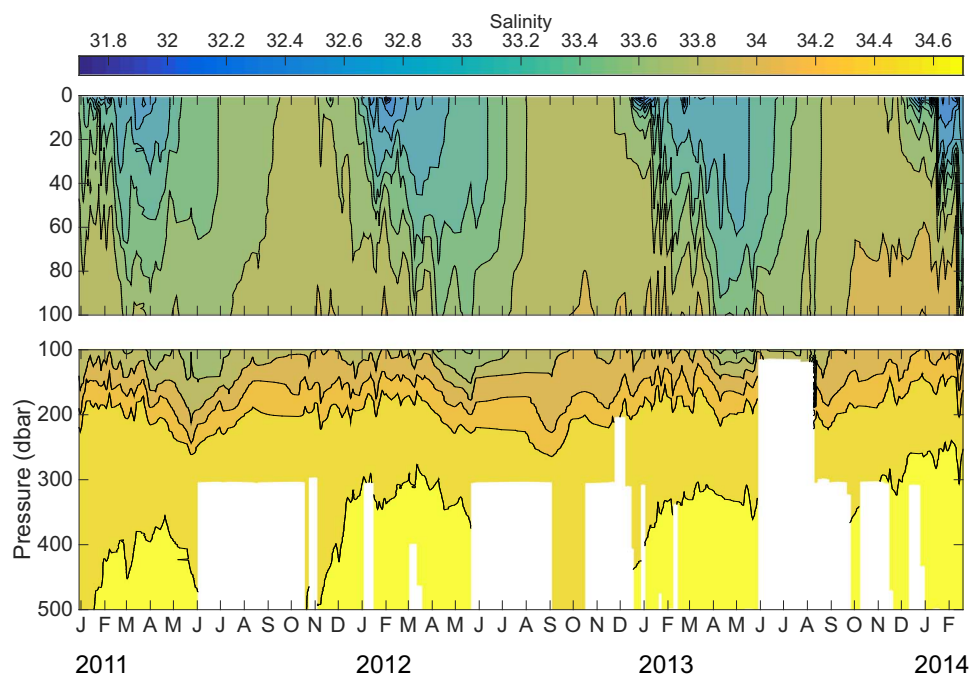

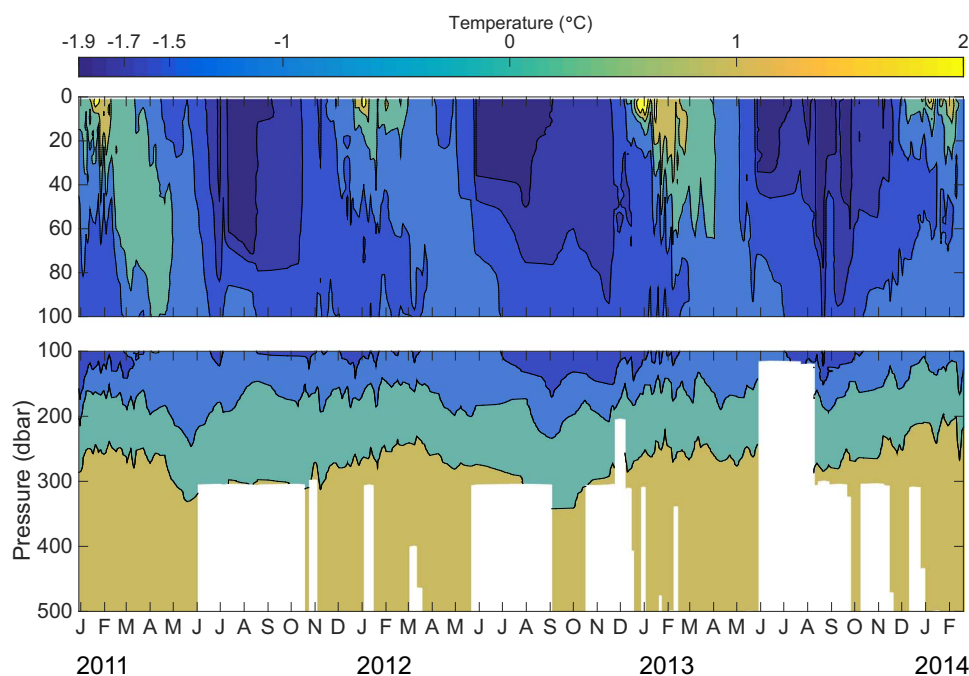**Fig. 10.** A full depth plot of salinity at RaTS site 1 during the carbon time series.

Fig. 11. A full depth plot of temperature at RaTS site 1 during the carbon time series.
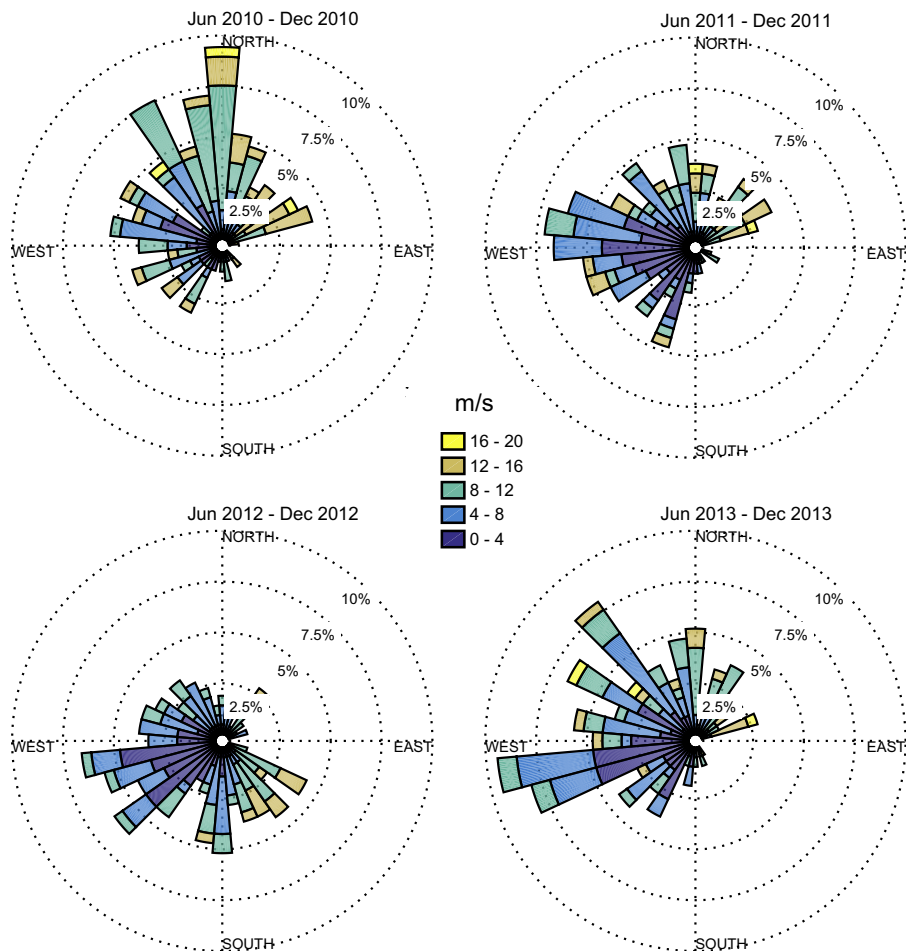
11

Fig. 12. Wind direction and speed (in m/s) for June–December in 2010–2013. Daily wind data from Rothera were taken from www.antarctica.ac.uk/met/metlog.

Appendix B. Accompanying data

See Figs. 10–12.

References

Arrigo, K., Mock, M., Lizotte, M.P., 2009. Primary producers and sea ice. In: Thomas, D. N., Dieckmann, G.S. (Eds.), Sea Ice, second edition. Wiley-Blackwell, Oxford, UK, pp. 283–326 (Chapter 8).

Arrigo, K.R., 2005. Marine microorganisms and global nutrient cycles. Nature 437, 349–355.

Bakker, D.C.E., Hoppema, M., Schroder, M., Geibert, W., de Baar, H.J.W., 2008. A rapid transition from ice covered CO_2 rich waters to a biologically mediated CO_2 sink in the eastern weddell gyre. Biogeosciences 5, 1373–1386.

Bednaršek, N., Tarling, G.A., Bakker, D.C.E., Fielding, S., Jones, E.M., Venables, H.J., Ward, P., Kuzirian, A., Lézé, B., Feely, R.A., Murphy, E.J., 2012. Extensive dissolution of live pteropods in the Southern Ocean. Nat. Geosci. 5, 881–885.

Bozec, Y., Thomas, H., Schiettecatte, L.s., Borges, A.V., Elkalay, K., de Baar, H.J.W., 2006. Assessment of the processes controlling seasonal variations of dissolved inorganic carbon in the North Sea. Limnol. Oceanogr. 51, 2746–2762.

Brewer, P.G., Goldman, J.C., 1976. Alkalinity changes generated by phytoplankton growth. Limnol. Oceanogr. 21, 108–117.

Brown, K.A., Miller, L.A., Davelaar, M., Francois, R., Tortell, P.D., 2014. Over-determination of the carbonate system in natural sea-ice brine and assessment of carbonic acid dissociation constants under low temperature, high salinity conditions. Mar. Chem. 165, 36–45.

Brzezinski, M.A., Dickson, M.L., Nelson, D.M., Sambrotto, R., 2003. Ratios of Si, C and N uptake by microplankton in the Southern Ocean. Deep Sea Res. Part II: Top. Stud. Oceanogr. 50, 619–633.

Carrillo, C.J., Smith, R.C., Karl, D.M., 2004. Processes regulating oxygen and carbon dioxide in surface waters west of the Antarctic Peninsula. Mar. Chem. 84, 161–179.

Chierici, M., Fransson, A., 2009. Calcium carbonate saturation in the surface water of the

Arctic Ocean: undersaturation in freshwater influenced shelves. Biogeosciences 6, 2421–2431.

Chierici, M., Fransson, A., Lansard, B., Miller, L.A., Mucci, A., Shadwick, E., Thomas, H., Tremblay, J.E., Papakyriakou, T.N., 2011. Impact of biogeochemical processes and environmental factors on the calcium carbonate saturation state in the circumpolar flaw lead in the Amundsen Gulf, Arctic Ocean. J. Geophys. Res. 116, C00G09.

Clarke, A., Meredith, M.P., Wallace, M.I., Brandon, M.A., Thomas, D.N., 2008. Seasonal and interannual variability in temperature, chlorophyll and macronutrients in Northern Marguerite Bay, Antarctica. Deep Sea Res. Part II: Top. Stud. Oceanogr. 55, 1988–2006.

Comeau, S., Jeffree, R., Teyssié, J.L., Gattuso, J.P., 2010. Response of the Arctic pteropod *Limacina helicina* to projected future environmental conditions. PloS One 5, e11362 .

Comiso, J.C., Nishio, F., 2008. Trends in the sea ice cover using enhanced and compatible AMSR-E, SSM/I, and SMMR data. J. Geophys. Res. 113, C02S07.

Cook, A.J., Fox, A.J., Vaughan, D.G., Ferrigno, J.G., 2005. Retreating glacier fronts on the Antarctic Peninsula over the past half-century. Science (New York,) 308, 541–544.

Delille, B., Vancoppenolle, M., Geilfus, N.-X., Tilbrook, B., Lannuzel, D., Schoemann, V., Becquevort, S., Carnat, G., Delille, D., Lancelot, C., Chou, L., Dieckmann, G.S., Tison, J.L., 2014. Southern Ocean CO_2 sink: the contribution of sea ice. J. Geophys. Res. Oceans 119, 6340–6355.

Dickson, A.G., Sabine, C.L., Christian, J.R., 2007. Guide to best practices for ocean CO_2 measurements. PICES Spec. Publ. 3, 191.

Dieckmann, G.S., Nehrke, G., Papadimitriou, S., Göttlicher, J., Steininger, R., Kennedy, H., Wolf-Gladrow, D., Thomas, D.N., 2008. Calcium carbonate as ikaite crystals in Antarctic sea ice. Geophys. Res. Lett. 35, L08501.

Egleston, E.S., Sabine, C.L., Morel, F.M.M., 2010. Revelle revisited: buffer factors that quantify the response of ocean chemistry to changes in DIC and alkalinity. Glob. Biogeochem. Cycl. 24, 1–9.

Feely, R.A., Sabine, C.L., Lee, K., Berelson, W., Kleypas, J., Fabry, V.J., Millero, F.J., 2004. Impact of anthropogenic CO_2 on the $CaCO_3$ system in the oceans. Science 305,

362–366.

Fransson, A., Chierici, M., Miller, L.A., Carnat, G., Shadwick, E., Thomas, H., Pineault, S., Papakyriakou, T.N., 2013. Impact of sea-ice processes on the carbonate system and ocean acidification at the ice–water interface of the Amundsen Gulf, Arctic Ocean. J. Geophys. Res.: Oceans 118, 7001–7023.

Geider, R., La Roche, J., 2002. Redfield revisited: variability of C:N:P in marine microalgae and its biochemical basis. Eur. J. Phycol. 37, 1–17.

Gibson, J.A.E., Trull, T.W., 1999. Annual cycle of fCO_2 under sea–ice and in open water in Prydz Bay, East Antarctica. Mar. Chem. 66, 187–200.

Goyet, C., Poisson, A., 1989. New determination of carbonic acid dissociation constants in seawater as a function of temperature and salinity. Deep-Sea Res. 36, 1635–1654.

Green, S.E., Sambrotto, R.N., 2006. Net community production in terms of C, N, P and Si in the Antarctic Circumpolar Current and its influence on regional water mass characteristics. Deep-Sea Res. Part I: Oceanogr. Res. Pap. 53, 111–135.

Hall, A., Visbeck, M., 2002. Synchronous variability in the Southern Hemisphere atmosphere, sea ice, and ocean resulting from the annular mode. J. Clim. 15, 3043–3057.

Hauri, C., Doney, S.C., Takahashi, T., Erickson, M., Jiang, G., Ducklow, H.W., 2015. Two decades of inorganic carbon dynamics along the Western Antarctic Peninsula. Biogeosciences 12, 6761–6779.

Henley, S.F., Ganeshram, R.S., Annett, A.L., Tuerena, R.E., Fallick, A.E., Meredith, M.P., Venables, H.J., Clarke, A. Macronutrient supply, uptake and recycling in the coastal ocean of the West Antarctic Peninsula. Deep Sea Res. Part II: Top. Stud. Oceanogr. (this issue).

Holland, P.R., Kwok, R., 2012. Wind-driven trends in Antarctic sea-ice drift. Nat. Geosci. 5, 872–875.

Hoppema, M., de Baar, H.J.W., Bellerby, R.G.J., Fahrbach, E., Bakker, K., 2002. Annual export production in the interior Weddell Gyre estimated from a chemical mass balance of nutrients. Deep-Sea Res. II 49, 1675–1689.

Johnson, K.M., King, A.E., Sieburth, J.M., 1985. Coulometric TCO_2 analyses for marine studies; an introduction. Mar. Chem. 16, 61–82.

Jones, E.M., Bakker, D.C.E., Venables, H.J., Whitehouse, M.J., Korb, R.E., Watson, A.J., 2010. Rapid changes in surface water carbonate chemistry during Antarctic sea ice melt. Tellus B 62B, 621–635.

Jones, E.M., Clargo, N., Fenton, M., Ossebaar, S., Venables, H.J., Meredith, M., de Baar, H.J.W., 2016. Carbonate system in Ryder Bay, West Antarctic Peninsula: regional patterns and processes. Deep Sea Res. Part II: Top. Stud. Oceanogr. (this issue).

Kawaguchi, S., Ishida, A., King, R., Raymond, B., Waller, N., Constable, A., Nicol, S., Wakita, M., Ishimatsu, A., 2013. Risk maps for Antarctic krill under projected southern ocean acidification. Nat. Clim. Change 3, 843–847.

Laws, E.A., 1991. Photosynthetic quotients, new production and net community production in the open ocean. Deep Sea Res. Part A: Oceanogr. Res. Pap. 38, 143–167.

Le Quéré, C., Rödenbeck, C., Buitenhuis, E.T., Conway, T.J., Langenfelds, R., Gomez, A., Labuschagne, C., Ramonet, M., Nakazawa, T., Metzl, N., Gillett, N., Heimann, M., 2007. Saturation of the Southern Ocean CO_2 sink due to recent climate change. Science 316, 2003–2006.

Legge, O.J., Bakker, D.C.E., Johnson, M.T., Meredith, M.P., Venables, H.J., Brown, P.J., Lee, G.A., 2015. The seasonal cycle of ocean-atmosphere CO_2 flux in Ryder Bay, West Antarctic Peninsula. Geophys. Res. Lett. 42, 2934–2942.

Lenton, A., Matear, R.J., 2007. Role of the Southern Annular Mode (SAM) in Southern Ocean CO_2 uptake. Global Biogeochem. Cycl., 21.

Lenton, A., Tilbrook, B., Law, R., Bakker, D.C.E., Doney, S.C., Gruber, N., Ishii, M., Hoppema, M., Lovenduski, N.S., Matear, R.J., McNeil, B.I., Metzl, N., Mikaloff Fletcher, S.E., Monteiro, P., Rödenbeck, C., Sweeney, C., Takahashi, T., 2013. Sea–air CO_2 fluxes in the Southern Ocean for the period 1990–2009. Biogeosciences 10, 4037–4054.

Lovenduski, N.S., Gruber, N., Doney, S.C., 2008. Toward a mechanistic understanding of the decadal trends in the Southern Ocean carbon sink. Global Biogeochem. Cycl., 22.

Manno, C., Morata, N., Primicerio, R., 2012. Limacina retroversa's response to combined effects of ocean acidification and sea water freshening. Estuar. Coast. Shelf Sci. 113, 163–171.

Marrari, M., Daly, K.L., Hu, C., 2008. Spatial and temporal variability of SeaWiFS chlorophyll a distributions west of the Antarctic Peninsula: implications for krill production. Deep-Sea Res. Part II: Top. Stud. Oceanogr. 55, 377–392.

Marshall, G.J., 2003. Trends in the southern annular mode from observations and re-analyses. J. Clim. 16, 4134–4143.

Marshall, G.J., Orr, A., van Lipzig, N.P.M., King, J.C., 2006. The impact of a changing southern hemisphere annular mode on Antarctic Peninsula summer temperatures. J. Clim. 19, 5388–5404.

Martiny, A.C., Vrugt, J.A., Primeau, F.W., Lomas, M.W., 2013. Regional variation in the particulate organic carbon to nitrogen ratio in the surface ocean. Glob. Biogeochem. Cycl. 27, 723–731.

Mattsdotter Björk, M., Fransson, A., Torstensson, A., Chierici, M., 2014. Ocean acidification state in western Antarctic surface waters: controls and interannual variability. Biogeosciences 11, 57–73.

McNeil, B.I., Matear, R.J., 2008. Southern Ocean acidification: a tipping point at 450-ppm atmospheric CO_2. Proc. Natl. Acad. Sci. USA 105, 18860–18864.

McNeil, B.I., Sweeney, C., Gibson, J.A.E., 2011. Short note: natural seasonal variability of aragonite saturation state within two antarctic coastal ocean sites. Antarct. Sci. 23, 411–412.

Meiners, K.M., Vancoppenolle, M., Thanassekos, S., Dieckmann, G.S., Thomas, D.N., Tison, J.L., Arrigo, K.R., Garrison, D.L., McMinn, A., Lannuzel, D., van der Merwe, P., Swadling, K.M., Smith, W.O., Melnikov, I., Raymond, B., 2012. Chlorophyll a in Antarctic sea ice from historical ice core data. Geophys. Res. Lett., 39.

Meredith, M.P., Brandon, M.A., Wallace, M.I., Clarke, A., Leng, M.J., Renfrew, I.A., van

Lipzig, N.P.M., King, J.C., 2008. Variability in the freshwater balance of Northern Marguerite Bay, Antarctic Peninsula: results from ^{18}O. Deep-Sea Res. Part II: Top. Stud. Oceanogr. 55, 309–322.

Meredith, M.P., King, J.C., 2005. Rapid climate change in the ocean west of the Antarctic Peninsula during the second half of the 20th century. Geophys. Res. Lett. 32, L19604.

Meredith, M.P., Renfrew, I.A., Clarke, A., King, J.C., Brandon, M.A., 2004. Impact of the 1997/98 ENSO on upper ocean characteristics in Marguerite Bay, western Antarctic Peninsula. J. Geophys. Res. 109, C09013.

Meredith, M.P., Stammerjohn, S.E., Venables, H.J., Ducklow, H.W., Martinson, D.G., Iannuzzi, R.A., Leng, M.J., Melchior, J., Wessem, V., Reijmer, C.H., Barrand, N.E., 2016. Changing distributions of sea ice melt and meteoric water west of the Antarctic Peninsula. Deep-Sea Res. Part II, 1–18, (this issue).

Meredith, M.P., Wallace, M.I., Stammerjohn, S.E., Renfrew, I.A., Clarke, A., Venables, H.J., Shoosmith, D.R., Souster, T., Leng, M.J., 2010. Changes in the freshwater composition of the upper ocean west of the Antarctic Peninsula during the first decade of the 21st century. Progr. Oceanogr. 87, 127–143.

Miller, L.A., Elliott, S., Papakyriakou, T., 2011. Sea ice biogeochemistry and material transport across the frozen interface. Oceanography 24, 202–218.

Millero, F.J., 2007. The marine inorganic carbon cycle. Chem. Rev. 107, 308–341.

Mintrop, L., Pérez, F.F., González, M., Magdalena, D.J., Körtzinger, C.A., 2000. Alkalinity determination by potentiometry: intercalibration using three different methods. Cienc. Mar. 26, 23–27.

Montes-Hugo, M., Doney, S.C., Ducklow, H.W., Fraser, W., Martinson, D., Stammerjohn, S.E., Schofield, O., 2009. Recent changes in phytoplankton communities associated with rapid regional climate change along the western Antarctic Peninsula. Science (New York) 323, 1470–1473.

Montes-Hugo, M., Sweeney, C., Doney, S.C., Ducklow, H., Frouin, R., Martinson, D.G., Stammerjohn, S., Schofield, O., 2010. Seasonal forcing of summer dissolved inorganic carbon and chlorophyll a on the western shelf of the Antarctic Peninsula. J. Geophys. Res. 115, C03024.

Moy, A.D., Howard, W.R., Bray, S.G., Trull, T.W., 2009. Reduced calcification in modern Southern Ocean planktonic foraminifera. Nat. Geosci. 2, 276–280.

Orr, J.C., Fabry, V.J., Aumont, O., Bopp, L., Doney, S.C., Feely, R.A., Gnanadesikan, A., Gruber, N., Ishida, A., Joos, F., Key, R.M., Lindsay, K., Maier-Reimer, E., Matear, R., Monfray, P., Mouchet, A., Najjar, R.G., Plattner, G.K., Rodgers, K.B., Sabine, C.L., Sarmiento, J.L., Schlitzer, R., Slater, R.D., Totterdell, I.J., Weirig, M.F., Yamanaka, Y., Yool, A., 2005. Anthropogenic ocean acidification over the twenty-first century and its impact on calcifying organisms. Nature 437, 681–686.

Parkinson, C.L., Cavalieri, D.J., 2012. Antarctic sea ice variability and trends, 1979–2010. Cryosphere 6, 871–880.

Quigg, A., Finkel, Z.V., Irwin, A.J., Rosenthal, Y., Ho, T.Y., Reinfelder, J.R., Schofield, O., Morel, F.M.M., Falkowski, P.G., 2003. Evolutionary inheritance of elemental stoichiometry in phytoplankton. Nature 425, 291–294.

Redfield, A.C., Ketchum, B.H., Richards, F.A., 1963. The influence of organisms on the composition of sea water. In: Hill, M. (Ed.), The Sea. John Wiley & Sons, New York, vol. 2, pp. 26–77.

Roden, N.P., Shadwick, E.H., Tilbrook, B., Trull, T.W., 2013. Annual cycle of carbonate chemistry and decadal change in Coastal Prydz Bay, East Antarctica. Mar. Chem. 155, 135–147.

Rubin, S.I., Takahashi, T., Chipman, D.W., Goddard, J.G., 1998. Primary productivity and nutrient utilization ratios in the Pacific sector of the Southern Ocean based on seasonal changes in seawater chemistry. Deep-Sea Res. I 45, 1211–1234.

Rysgaard, S., Bendtsen, J., Delille, B., Dieckmann, G.S., Glud, R.N., Kennedy, H., Mortensen, J., Papadimitriou, S., Thomas, D.N., Tison, J.L., 2011. Sea ice contribution to the air–sea CO_2 exchange in the Arctic and Southern oceans. Tellus B 63, 823–830.

Rysgaard, S., Glud, R.N., Sejr, M.K., Bendtsen, J., Christensen, P.B., 2007. Inorganic carbon transport during sea ice growth and decay: a carbon pump in polar seas. J. Geophys. Res. 112, C03016.

Sabine, C.L., Feely, R.A., Gruber, N., Key, R.M., Lee, K., Bullister, J.L., Wanninkhof, R., Wong, C.S., Wallace, D.W.R., Tilbrook, B., Millero, F.J., Peng, T.H., Kozyr, A., 2004. The oceanic sink for anthropogenic CO_2. Science 305, 367–371.

Sallée, J.B., Matear, R.J., Rintoul, S.R., Lenton, A., 2012. Localized subduction of anthropogenic carbon dioxide in the southern hemisphere oceans. Nat. Geosci. 5, 579–584.

Sambrotto, R.N., Savidge, G., Robinson, C., Boyd, P., Takahashi, T., Karl, D.M., Langdon, C., Chipman, D., Marra, J., Codispoti, L., 1993. Elevated consumption of carbon relative to nitrogen in the surface ocean. Nature 363, 248–250.

Shadwick, E.H., Thomas, H., Chierici, M., Else, B., Fransson, A., Michel, C., Miller, L.A., Mucci, A., Niemi, A., Papakyriakou, T.N., Tremblay, J.É, 2011. Seasonal variability of the inorganic carbon system in the Amundsen Gulf region of the southeastern Beaufort sea. Limnol. Oceanogr. 56, 303–322.

Shadwick, E.H., Trull, T.W., Thomas, H., Gibson, J.A.E., 2013. Vulnerability of polar oceans to anthropogenic acidification: comparison of Arctic and Antarctic seasonal cycles. Sci. Rep. 3, 2339.

Stammerjohn, S.E., Martinson, D.G., Smith, R.C., Yuan, X., Rind, D., 2008. Trends in antarctic annual sea ice retreat and advance and their relation to El Niño Southern Oscillation and Southern Annular Mode variability. J. Geophys. Res. 113, C03S90.

Sweeney, C., 2003. The annual cycle of surface water CO_2 and O_2 in the Ross Sea,: a model for gas exchange on the continental shelves of Antarctica. Antarc. Res. Ser. 78, 295–312.

Thomas, H., Ittekkot, V., Osterroht, C., Schneider, B., 1999. Preferential recycling of nutrients – The ocean's way to increase new production and to pass nutrient limitation? Limnol. Oceanogr. 44, 1999–2004.

Thompson, D.W.J., Solomon, S., 2002. Interpretation of recent southern hemisphere

climate change. Science 296, 895–899.

Tortell, P.D., Bittig, H.C., Körtzinger, A., Jones, E.M., Hoppema, M., 2015. Biological and physical controls on N_2, O_2, and CO_2 distributions in contrasting Southern Ocean surface waters. Glob. Biogeochem. Cycl. 29, 994–1013.

Turner, J., Colwell, S.R., Marshall, G.J., Lachlan-Cope, T.A., Carleton, A.M., Jones, P.D., Lagun, V., Reid, P.A., Iagovkina, S., 2005. Antarctic climate change during the last 50 years. Int. J. Climatol. 25, 279–294.

Van Heuven, S., Pierrot, D., Rae, J.W.B., Lewis, E., Wallace, D.W.R., 2011. MATLAB Program Developed for CO_2 System Calculations, ORNL/CDIAC-105b. Carbon Dioxide Information Analysis Center, Oak Ridge National Laboratory, U.S .Department of Energy, Oak Ridge, Tennessee.

Vaughan, D.G., Marshall, G.J., Connolley, W.M., Parkinson, C., Mulvaney, R., Hodgson, D.A., King, J.C., Pudsey, C.J., Turner, J., 2003. Recent rapid regional climate warming on the Antarctic Peninsula. Clim. Change 60, 243–274.

Venables, H.J., Clarke, A., Meredith, M.P., 2013. Wintertime controls on summer stratification and productivity at the Western Antarctic Peninsula. Limnol. Oceanogr. 58, 1035–1047.

Venables, H.J., Meredith, M.P., 2014. Feedbacks between ice cover, ocean stratification, and heat content in Ryder Bay, West Antarctic Peninsula. J. Geophys. Res. Oceans 119, 5323–5336.

Vernet, M., Martinson, D., Iannuzzi, R., Stammerjohn, S., Kozlowski, W., Sines, K., Smith, R., Garibotti, I., 2008. Primary production within the sea-ice zone west of the Antarctic Peninsula: sea ice, summer mixed layer, and irradiance. Deep Sea Res. Part II: Top. Stud. Oceanogr. 55, 2068–2085.

Wanninkhof, R., Park, G.H., Takahashi, T., Sweeney, C., Feely, R., Nojiri, Y., Gruber, N., Doney, S.C., McKinley, G.A., Lenton, A., Le Quéré, C., Heinze, C., Schwinger, J., Graven, H., Khatiwala, S., 2013. Global ocean carbon uptake: magnitude, variability and trends. Biogeosciences 10, 1983–2000.

Weston, K., Jickells, T.D., Carson, D.S., Clarke, A., Meredith, M.P., Brandon, M.A., Wallace, M.I., Ussher, S.J., Hendry, K.R., 2013. Primary production export flux in Marguerite Bay (Antarctic Peninsula): linking upper water-column production to sediment trap flux. Deep Sea Res. Part I: Oceanogr. Res. Pap. 75, 52–66.

Yamamoto-Kawai, M., Mclaughlin, F.A., Carmack, E.C., Nishino, S., Shimada, K., 2009. Aragonite undersaturation in the Arctic Ocean: effects of ocean acidification and sea ice melt. Science 326, 1098–1100.

Zeebe, R.E., Wolf-Gladrow, D.A., 2001. CO_2 in Seawater: Equilibrium, Kinetics, Isotopes, Elsevier Oceanography Series, Elsevier, Amsterdam, vol. 65, pp. 346.